

Dissociation Energy of the Hydrogen Molecule at 10^{-9} Accuracy

C.-F. Cheng, J. Hussels, M. Niu, H. L. Bethlem, K. S. E. Eikema, E. J. Salumbides, and W. Ubachs*
*Department of Physics and Astronomy, LaserLab, Vrije Universiteit Amsterdam,
 de Boelelaan 1081, 1081 HV Amsterdam, The Netherlands*

M. Beyer, N. Hölsch, J. A. Agner, and F. Merkt
Laboratorium für Physikalische Chemie, ETH Zürich, 8093 Zürich, Switzerland

L.-G. Tao and S.-M. Hu
*Hefei National Laboratory for Physical Sciences at Microscale, iChem center,
 University of Science and Technology China, Hefei, 230026 China*

Ch. Jungen
*Laboratoire Aimé Cotton du CNRS, Bâtiment 505, Université de Paris-Sud, F-91405 Orsay, France
 and Department of Physics and Astronomy, University College London, London WC1E 6BT, United Kingdom*



(Received 19 March 2018; published 3 July 2018; corrected 9 July 2018)

The ionization energy of ortho- H_2 has been determined to be $E_1^o(H_2)/(hc) = 124\,357.238\,062(25)$ cm^{-1} from measurements of the $GK(1, 1) - X(0, 1)$ interval by Doppler-free, two-photon spectroscopy using a narrow band 179-nm laser source and the ionization energy of the $GK(1, 1)$ state by continuous-wave, near-infrared laser spectroscopy. $E_1^o(H_2)$ was used to derive the dissociation energy of H_2 , $D_0^{N=1}(H_2)$, at $35\,999.582\,894(25)$ cm^{-1} with a precision that is more than one order of magnitude better than all previous results. The new result challenges calculations of this quantity and represents a benchmark value for future relativistic and QED calculations of molecular energies.

DOI: [10.1103/PhysRevLett.121.013001](https://doi.org/10.1103/PhysRevLett.121.013001)

The dissociation energy of the hydrogen molecule $D_0(H_2)$ is a fundamental quantity for testing molecular quantum theory. The pioneering calculations of Heitler and London on H_2 demonstrated that molecular binding is a consequence of quantum mechanics [1]. In almost a century of mutually stimulating activities by experimentalists and theorists, the accuracy of this benchmark value has been improved by seven orders of magnitude [2]. Great progress in the theoretical calculations has been achieved by including relativistic and quantum-electrodynamic (QED) effects [3,4]. Over the past decade, improved calculations of the Born-Oppenheimer energies [5], adiabatic corrections [6], leading-order nonadiabatic corrections [7], exact nonadiabatic energies [8,9], and a further refinement of QED calculations [10] have been reported. The latest efforts, however, led to a deterioration of the agreement between experimental and theoretical results [11].

Direct measurements of dissociation energies in H_2 are complicated by perturbing resonances near the continuum limits and vanishing direct photodissociation cross sections at the thresholds [12,13]. Such difficulties can be overcome by a measurement of the adiabatic ionization energy $E_1(H_2)$ combined with a thermodynamic cycle involving the ionization energy of atomic hydrogen $E_1(H)$ and the dissociation energy of the molecular ion $D_0(H_2^+)$ [14] via

$$D_0(H_2) = E_1(H_2) + D_0(H_2^+) - E_1(H),$$

as illustrated in Fig. 1. The dissociation energies $D_0^{N=1}$ and $D_0^{N=0}$ of ortho- and para- H_2 differ by the rotational term value of the $X(v=0, N=1)$ level, i.e., $118.48\,684(10)$ cm^{-1} [15].

The most accurate previous determination of $D_0(H_2)$, at a relative accuracy of 10^{-8} [16], involved two-photon Doppler-free laser excitation to the $EF\ ^1\Sigma_g^+(v=0, N=1)$ intermediate state [17], one-photon ultraviolet excitation from the $EF\ ^1\Sigma_g^+(0, 1)$ to the $56p1_1$ Rydberg state [16], and millimeter wave (MMW) spectroscopy of high-lying Rydberg states [18], allowing for an extrapolation to the ionization energy by multichannel quantum-defect theory (MQDT) [19]. The initial $EF-X$ step in this scheme has recently been improved by two orders of magnitude to an accuracy of 73 kHz [20], but an improvement of $D_0(H_2)$ awaits an improved measurement of the $EF-np$ interval.

In the present Letter, we adopt an alternative excitation scheme to determine $D_0(H_2)$, through the $GK\ ^1\Sigma_g^+(1, 1)$ intermediate state, which offers the possibility of using continuous-wave (cw) near-infrared (NIR) laser excitation to high- n Rydberg states [21]. Experimental results from two laboratories are combined: the measurement of the Doppler-free two-photon transition $GK(1, 1) \leftarrow X(0, 1)$ in

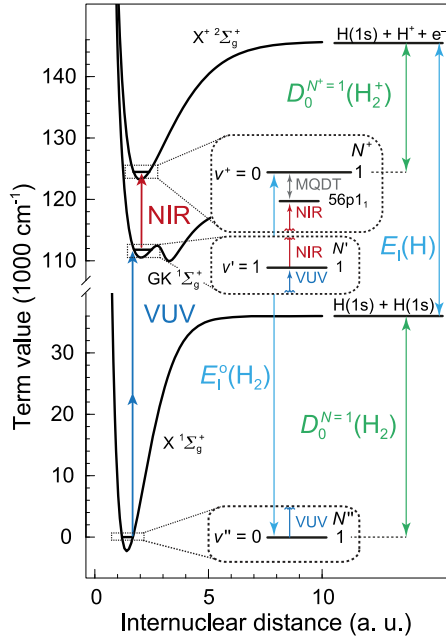


FIG. 1. Potential energy diagram of electronic states in molecular hydrogen relevant to this Letter.

Amsterdam, and the determination of the interval between $GK(1,1)$ and the $56p1_1$ Rydberg state by NIR cw-laser spectroscopy in Zürich.

In the $GK-X$ experiment, schematically depicted in Fig. 2, a narrow bandwidth (~ 9 MHz) injection-seeded oscillator-amplifier titanium sapphire (Ti:Sa) laser system delivers 50-ns-long pulses at the fundamental wavelength of 716 nm. The amplified pulsed output is frequency up-converted in two doubling stages, with BBO and $KBe_2BO_3F_2$ (KBBF) crystals, leading to the generation of 179-nm radiation to drive the $GK(1,1) \leftarrow X(0,1)$ transition in a two-photon scheme. The vacuum-ultraviolet (VUV) output power of $20 \mu J$ per pulse is limited by the optical damage threshold of the KBBF crystal [22]. A glass pinhole with a diameter of 0.5 mm is employed to align the reflected beam in a counter-propagating Doppler-free configuration. A separate 633-nm pulsed dye laser is used to ionize the molecules from the $GK(1,1)$ state in a single-photon ionization process. To reduce ac Stark effects, this laser is delayed by 30 ns with respect to the 179-nm pulse. Further increase of the delay is detrimental because the lifetime of the $GK(1,1)$ state is $24(3)$ ns [23]. The H_2^+ ions are collected and detected by the velocity-map-imaging method [24].

The cw Ti:Sa laser, which has a short-term (one second) frequency stability of a few tens of kHz, is locked to an optical frequency comb, resulting in a long-term relative accuracy better than 10^{-12} . An acousto-optic modulator (AOM) was implemented in a double-pass scheme to scan the cw laser frequency, the output of which is used as a seed for the oscillator cavity. The frequency offset, or chirp,

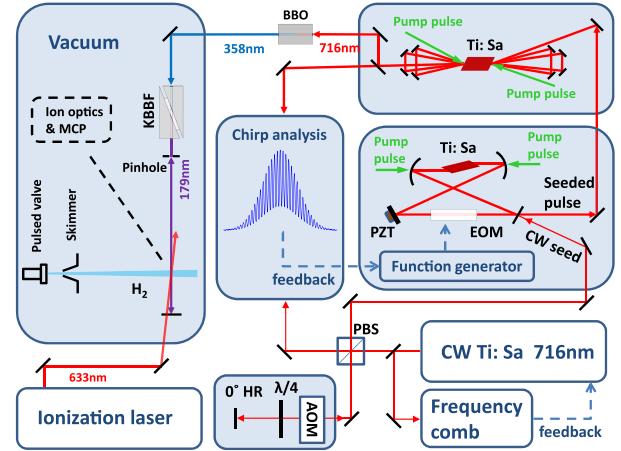


FIG. 2. Schematic layout of the $GK-X$ experimental setup, where the pulsed pump laser for the oscillator and amplifier is not shown.

between the pulsed output and the cw seed was measured for each pulse [17]. An intracavity electro-optic phase modulator (EOM), driven by an arbitrary function generator, is used for active frequency chirp compensation, as shown in Fig. 2. In addition, the residual chirp value is recorded and corrected at each frequency scan step. An upper limit of the systematic uncertainty associated with chirp is extracted from the statistical analysis, by repeating the measurements after changing the antichirp parameters.

A typical scan is shown in Fig. 3(a), with 50-shot averaging for each frequency scan step. The observed two-photon transition linewidth is dominated by the laser bandwidth, with a small contribution of the natural linewidth ($\Gamma = 6.6$ MHz). An imperfect counter-propagating alignment may result in a residual first-order Doppler shift. This was quantified by performing velocity-dependent measurements using various mixtures of H_2 and Ne, and extrapolating to a zero-velocity transition frequency, as shown in Fig. 3(b). Several measurements were performed using different alignment configurations of the counter-propagating VUV laser beams. After accounting for the second-order Doppler shift, which is $150(30)$ kHz in pure H_2 with a velocity of $2900(300)$ m/s, a global fitting procedure is applied, where the zero-velocity intercept is shared for all alignment settings. The extrapolation yields the Doppler-free transition frequency with a systematic uncertainty of 350 kHz, which is the largest contribution to the error budget. The normalized velocity of the H_2 beam in Fig. 3 is defined as $v_{\text{norm}} = v_{\text{mix}}/v_{\text{pure}} = \sqrt{m_{H_2}/(n_{H_2}m_{H_2} + n_{Ne}m_{Ne})}$, where n_{H_2} and n_{Ne} are the mixture fractions of H_2 and Ne, and m_{H_2} and m_{Ne} are their masses [25].

The ac Stark effect for both the 179-nm and the ionization lasers was studied by performing intensity-dependent measurements. Typically the 179-nm laser power was fixed to $2 \mu J$ per pulse during the residual

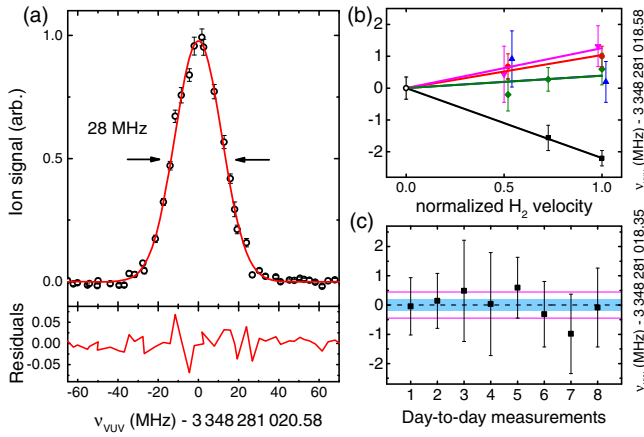


FIG. 3. (a) Recording of a $GK(1,1) \leftarrow X(0,1)$ transition in H_2 (black circles). The red line is a fitted Gaussian curve with the residuals shown below. (b) Assessment of the residual first-order Doppler effect. Each color indicates an individual alignment configuration, where the largest deliberate misalignment is about 0.3 mrad. The blue and magenta points are shifted by 0.02 and -0.02 in velocity axis for clarity. The colored lines show a linear global fit for all alignments, resulting in the Doppler-free value indicated with the open circle. (c) Transition frequency measurements in different days. Each point indicates an average value for one day with its standard deviation. The dash line shows the mean value. The magenta line and the cyan area give the standard deviation of the data and of the mean, respectively, where the former is taken as a conservative statistical uncertainty.

Doppler-shift determination, while up to $10 \mu\text{J}$ was generated to assess the ac Stark effect. A similar procedure is applied for the ionization laser, including the assessment of systematic shifts caused by the temporal overlap between

the two laser pulses. The Doppler-extrapolated value was corrected for the ac Stark shifts. Other possible systematic and statistical uncertainties were derived from day-to-day frequency differences (215 measurements in total) over several days [see Fig. 3(c)]. The uncertainty budget is given in Table I, and the combined statistical and systematic uncertainty of the $GK-X$ transition is 650 kHz, corresponding to a relative accuracy of 2×10^{-10} .

The interval between the $GK(1,1)$ state and the $56p1_1(v^+ = 0, S = 0, F = 0-2)$ Rydberg state of ortho- H_2 was measured using the same apparatus, laser setup, and calibration procedure as described in detail in a recent article presenting a measurement of the $50f0_3 \leftarrow GK(0,2)$ interval [21]. The measurement was carried out using a pulsed and skimmed supersonic beam of pure H_2 , and the procedure involved (i) the compensation of the stray electric fields in three dimensions to better than 1 mV/cm, which limits possible Stark shifts to below 7 kHz for the $56p1_1$ level [26], (ii) shielding external magnetic fields so that the maximal Zeeman shifts are below 10 kHz, (iii) the cancellation of the first-order Doppler shift to better than 110 kHz by performing the excitation with the NIR-laser beam of 792-nm wavelength and its back reflection overlapped to better than 0.05 mrad and averaging the central frequencies of both Doppler components [see Fig. 4(a)]—repeating the measurements after a full alignment of the laser and molecular beams transforms the systematic uncertainty associated with the residual Doppler shift into a statistical uncertainty—(iv) cooling the valve used to generate the supersonic beam to 80 K, thus reducing the mean beam velocity to 1290(20) m/s and leading to a second-order Doppler shift of $-4.1(5)$ kHz, and (v) calibrating the

TABLE I. Transition frequencies of H_2 and their uncertainties.

Transition	$GK(1,1) \leftarrow X(0,1)$		$56p1_1 \leftarrow GK(1,1)$	
Measured frequency	3 348 281 018.58(49) MHz		378 809 479.24(30) MHz	
Effect	Correction	Uncertainty	Correction	Uncertainty
dc Stark shift		< 10 kHz		7 kHz
ac Stark shift	-40 kHz	90 kHz, ^a		4 kHz
	-190 kHz	200 kHz, ^b		
Chirp		(< 490 kHz) _{stat} , ^c	...	
Zeeman shift		< 10 kHz		10 kHz
Collision shift		< 1 kHz		1 kHz
Residual first-order Doppler shift		350 kHz		(< 110 kHz) _{stat} , ^c
Second-order Doppler shift		< 30 kHz, ^d	+4.1 kHz	0.5 kHz
Line shape model	...			200 kHz
Hyperfine structure (c.g. shift)		< 100 kHz		100 kHz
Photon-recoil-shift correction	...		-160 kHz	
Total systematic uncertainty		426 kHz		224 kHz
Final frequency	3 348 281 018.35(49) _{stat} (43) _{sys} MHz		378 809 479.08(30) _{stat} (22) _{sys} MHz	

^aFor the ionization laser.

^bFor the VUV laser.

^cThis systematic uncertainty is already included in the statistical uncertainty of the frequency measurements.

^dThe second-order Doppler shift values are subtracted for different velocities in Fig. 3(b) and the error is included in the residual first-order Doppler shift uncertainty.

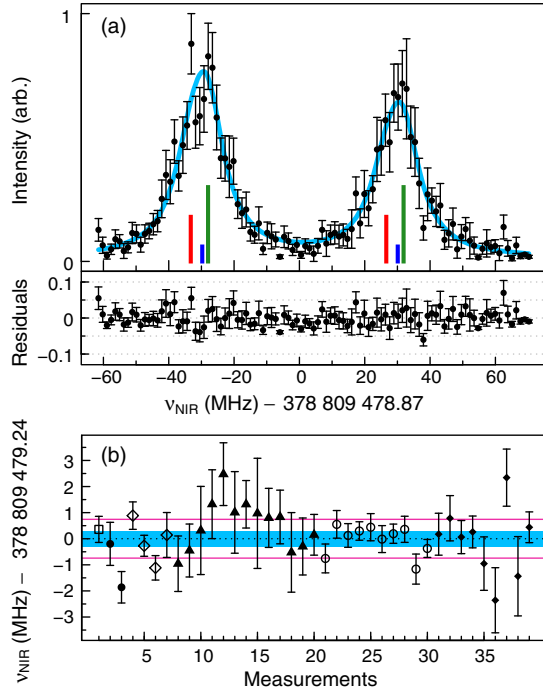


FIG. 4. (a) Typical spectrum of the $56p1_1 \leftarrow GK(1,1)$ transition of H_2 and its analysis based on a Lorentzian line shape model and the hyperfine structure of the $56p1_1$ Rydberg state given as red ($F = 1$), blue ($F = 0$), and green ($F = 2$) sticks. The weighted residuals are depicted below the spectrum. (b) Doppler-free frequencies with standard deviations of individual measurements. The magenta line and the cyan area give the standard deviation of the full data set and of the mean, respectively. The symbols label measurements carried out on different days.

excitation frequency with a frequency comb referenced to a 10-MHz Rb oscillator (Stanford Research Systems, FS275).

A typical individual spectrum is displayed in Fig. 4(a) as dots with error bars. The figure also depicts a fit of a model line shape consisting of two Doppler components. Each of these is the sum of three hyperfine components (stick spectrum) having the same Lorentzian width, intensities given by their statistical weights of $2F + 1$, and relative positions corresponding to those measured by millimeter-wave spectroscopy [2,18]. In the fit, the data points were weighted by taking into account the Poissonian statistics of the ion counts and the background noise as explained in

Ref. [21]. The central positions determined from 39 measurements are plotted in Fig. 4(b) with their statistical uncertainties. Their weighted mean, indicated by the dashed line, is 378 809 479.24(30) MHz, where the statistical uncertainty of 300 kHz corresponds to $\bar{\sigma} = \sigma/\sqrt{N}$, N being the number of independent measurements, which we took to be the number of measurement sets recorded on different days rather than the number of individual measurements (i.e., 6, as indicated by the different symbols in Fig. 4(b), rather than 39).

The systematic uncertainties considered in the analysis are summarized in Table I and sum up to 224 kHz, dominated by the uncertainty resulting from the possible deviations from a statistical intensity distribution of the unresolved hyperfine structure of the $56p1_1 \leftarrow GK(1,1)$ line (Line shape model entry in Table I). After subtraction of the photon recoil shift of 160 kHz, our final result for the $56p1_1 \leftarrow GK(1,1)$ interval is shown in Table I. This value is consistent with, but four times more precise than, the value of 378 809 478.7(12) MHz reported in [26].

The experimental values of the $56p1_1 \leftarrow GK(1,1)$ interval in Table I correspond to the center of gravity (c.g.) of the hyperfine components. The hyperfine splitting of the $GK(1,1)$ state, which has d character, is estimated to be 330 kHz from the known hyperfine structure of high- nd Rydberg states [18] and leads to a systematic uncertainty contribution of 100 kHz for the transition center frequency. In addition, the hyperfine splitting of the $X(0,1)$ state, which was observed by Ramsey to be 600 kHz [27], also contributes to the systematic uncertainty for the $GK(1,1) \leftarrow X(0,1)$ measurement. In the center-of-gravity transition frequency determination, a contribution of less than 100 kHz is estimated.

The binding energy of the $56p1_1$ Rydberg state with respect to the first rovibronic state $X^+(v^+ = 0, N^+ = 1)$ of ortho- H_2^+ was determined via a MQDT-assisted fitting procedure applied to 76 measured np hyperfine components with $54 < n < 64$, as described in Ref. [28] and the value is given in Table II. Combining all contributions, the ionization energy of ortho- H_2 , $E_1^o(H_2)$, is determined to be 124 357.238 062(25) cm^{-1} (see Table II), corresponding to a relative accuracy of 2×10^{-10} . The dissociation energy, $D_0^{N=1}(H_2)$, is derived from $E_1^o(H_2)$ to be

TABLE II. Energy level intervals and determination of the ionization E_1 and dissociation energies D_0 of ortho- H_2 (in cm^{-1}).

	Energy level interval	Value	Reference	Comment
(1)	$GK(v = 1, N = 1) - X(v = 0, N = 1)$	111 686.632 836(22)	This Letter	
(2)	$56p1_1(v^+ = 0, S = 0, \text{center}) - GK(v = 1, N = 1)$	12 635.724 114(12)	This Letter	
(3)	$X^+(v^+ = 0, N^+ = 1, \text{center}) - 56p1_1(v^+ = 0, S = 0, \text{center})$	34.881 112(5)	[28]	
(4)	$[H(1s) + H^+] - X^+(v^+ = 0, N^+ = 1, \text{center})$	21 321.116 575 5(6)	[29,30]	$D_0^{N^+=1}(H_2^+)$
(5)	$[H(1s) + H^+] - [H(1s) + H(1s)]$	109 678.771 743 07(10)	[30]	$E_1(H)$
(6)	(1) + (2) + (3)	124 357.238 062(25)	This Letter	$E_1^o(H_2)$
(7)	(1) + (2) + (3) + (4) - (5)	35 999.582 894(25)	This Letter	$D_0^{N=1}(H_2)$

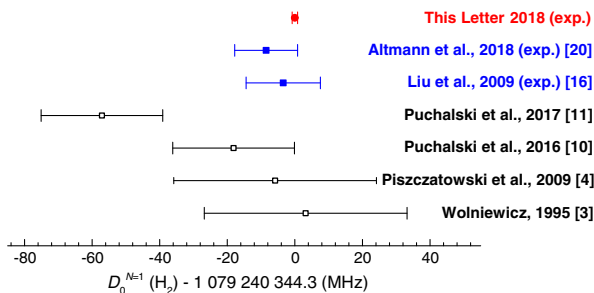


FIG. 5. Comparison between experimental and theoretical values of $D_0^{N=1}$ for ortho- H_2 .

$35\,999.582\,894(25)\text{ cm}^{-1}$ or $1\,079\,240\,344.3(8)\text{ MHz}$ with a relative accuracy of 7×10^{-10} , by using the values of $D_0^{N=1}(H_2^+)$, calculated to an accuracy of $6 \times 10^{-7}\text{ cm}^{-1}$ [29,30], and $E_1(H)$, which is included in the CODATA 2014 recommended values [30].

A comparison between our new value of $D_0^{N=1}(H_2)$ and the most recent experimental and theoretical results is presented in Fig. 5. Our result confirms the validity of the previous experimental result [16] using a different excitation sequence, but it improves its accuracy by one order of magnitude. It deviates from the newest theoretical result reported in Ref. [11] by more than three times the uncertainty. Possible reasons for the discrepancy between the experimental and theoretical values of $D_0(H_2)$ include the underestimation of nonadiabatic effects in the determination of the relativistic and QED corrections to $D_0(H_2)$ [11], or a more fundamental problem in the molecular quantum theory. Resolving this puzzle and further improvement of this value to 10-kHz accuracy, for both experiment and theory, will open a new route for determining the proton charge radius [11,31] with 1% accuracy, or an improved value of the proton-to-electron mass ratio [32,33].

F. M. and W. U. acknowledge the European Research Council for an ERC-Advanced grant under the European Union’s Horizon 2020 research and innovation programme (Grant agreement No. 670168 and No. 743121). The project is funded by Laserlab-Europe EU-H2020 654148. H. B., K. E., and W. U. acknowledge FOM/NWO for a program grant on “The Mysterious Size of the Proton.” F. M. acknowledges the Swiss National Science Foundation (Project No. 200020-172620). S. H. acknowledges the support from NSFC (21688102) and CAS (XDB21020100).

*w.m.g.ubachs@vu.nl

- [1] W. Heitler and F. London, *Z. Phys.* **44**, 455 (1927).
- [2] D. Sprecher, C. Jungen, W. Ubachs, and F. Merkt, *Faraday Discuss. Chem. Soc.* **150**, 51 (2011).
- [3] L. Wolniewicz, *J. Chem. Phys.* **103**, 1792 (1995).
- [4] K. Piszczatowski, G. Łach, M. Przybytek, J. Komasa, K. Pachucki, and B. Jeziorski, *J. Chem. Theory Comput.* **5**, 3039 (2009).

- [5] K. Pachucki, *Phys. Rev. A* **82**, 032509 (2010).
- [6] K. Pachucki and J. Komasa, *J. Chem. Phys.* **141**, 224103 (2014).
- [7] K. Pachucki and J. Komasa, *J. Chem. Phys.* **143**, 034111 (2015).
- [8] K. Pachucki and J. Komasa, *J. Chem. Phys.* **144**, 164306 (2016).
- [9] B. Simmen, E. Mátyus, and M. Reiher, *Mol. Phys.* **111**, 2086 (2013).
- [10] M. Puchalski, J. Komasa, P. Czachorowski, and K. Pachucki, *Phys. Rev. Lett.* **117**, 263002 (2016).
- [11] M. Puchalski, J. Komasa, and K. Pachucki, *Phys. Rev. A* **95**, 052506 (2017).
- [12] G. Herzberg, *J. Mol. Spectrosc.* **33**, 147 (1970).
- [13] Y. P. Zhang, C. H. Cheng, J. T. Kim, J. Stanojevic, and E. E. Eyler, *Phys. Rev. Lett.* **92**, 203003 (2004).
- [14] G. Herzberg and C. Jungen, *J. Mol. Spectrosc.* **41**, 425 (1972).
- [15] D. E. Jennings, S. L. Bragg, and J. W. Brault, *Astrophys. J. Lett.* **282**, L85 (1984).
- [16] J. Liu, E. J. Salumbides, U. Hollenstein, J. C. J. Koelemeij, K. S. E. Eikema, W. Ubachs, and F. Merkt, *J. Chem. Phys.* **130**, 174306 (2009).
- [17] S. Hannemann, E. J. Salumbides, S. Witte, R. T. Zinkstok, E. J. van Duijn, K. S. E. Eikema, and W. Ubachs, *Phys. Rev. A* **74**, 062514 (2006).
- [18] A. Osterwalder, A. Wüest, F. Merkt, and C. Jungen, *J. Chem. Phys.* **121**, 11810 (2004).
- [19] C. Haase, M. Beyer, C. Jungen, and F. Merkt, *J. Chem. Phys.* **142**, 064310 (2015).
- [20] R. K. Altmann, L. S. Dreissen, E. J. Salumbides, W. Ubachs, and K. S. E. Eikema, *Phys. Rev. Lett.* **120**, 043204 (2018).
- [21] M. Beyer, N. Hölsch, J. A. Agner, J. Deiglmayr, H. Schmutz, and F. Merkt, *Phys. Rev. A* **97**, 012501 (2018).
- [22] H. Zhang, G. Wang, L. Guo, A. Geng, Y. Bo, D. Cui, Z. Xu, R. Li, Y. Zhu, X. Wang *et al.*, *Appl. Phys. B* **93**, 323 (2008).
- [23] S. A. Astashkevich and B. P. Lavrov, *J. Phys. Chem. Ref. Data* **44**, 023105 (2015).
- [24] A. T. J. B. Eppink and D. H. Parker, *Rev. Sci. Instrum.* **68**, 3477 (1997).
- [25] G. Scoles, D. Bassi, U. Buck, and D. Lainé, *Atomic and Molecular Beam Methods* (Oxford University Press, New York, 1988).
- [26] D. Sprecher, M. Beyer, and F. Merkt, *Mol. Phys.* **111**, 2100 (2013).
- [27] N. F. Ramsey, *Phys. Rev.* **85**, 60 (1952).
- [28] D. Sprecher, C. Jungen, and F. Merkt, *J. Chem. Phys.* **140**, 104303 (2014).
- [29] V. I. Korobov, L. Hilico, and J.-P. Karr, *Phys. Rev. Lett.* **118**, 233001 (2017).
- [30] P. J. Mohr, D. B. Newell, and B. N. Taylor, *Rev. Mod. Phys.* **88**, 035009 (2016).
- [31] R. Pohl, A. Antognini, F. Nez, F. D. Amaro, F. Biraben, J. M. R. Cardoso, D. S. Covita, A. Dax, S. Dhawan, L. M. P. Fernandes *et al.*, *Nature (London)* **466**, 213 (2010).
- [32] W. Ubachs, J. C. J. Koelemeij, K. S. E. Eikema, and E. J. Salumbides, *J. Mol. Spectrosc.* **320**, 1 (2016).
- [33] L. G. Tao, A. W. Liu, K. Pachucki, J. Komasa, Y. R. Sun, J. Wang, and S. M. Hu, *Phys. Rev. Lett.* **120**, 153001 (2018).

Correction: An interior label in Fig. 5 was misset and has been fixed.